Published online 7 May 2020 *Nucleic Acids Research, 2020, Vol. 48, No. 11* **6019–6031**
doi: 10.1093/nar/gkaa224

A critical role of telomere chromatin compaction in ALT tumor cell growth

Guang Shi[1,2,†], Yang Hu[1,†], Xing Zhu[1], Yuanling Jiang[1], Junjie Pang[1], Chuanle Wang[1], Wenjun Huang[1], Yong Zhao[1], Wenbin Ma[1], Dan Liu[3], Junjiu Huang[1,2,4,*] and Zhou Songyang[1,2,3,4,*]

[1]MOE Key Laboratory of Gene Function and Regulation, Guangzhou Key Laboratory of Healthy Aging Research and SYSU-BCM Joint Research Center, School of Life Sciences, Sun Yat-sen University, Guangzhou 510275, China, [2]Sun Yat-sen Memorial Hospital, Sun Yat-sen University, Guangzhou 510120, China, [3]Verna and Marrs Mclean Department of Biochemistry and Molecular Biology, Baylor College of Medicine, One Baylor Plaza, Houston, TX, USA 77030 and [4]State Key Laboratory of Ophthalmology, Zhongshan Ophthalmic Center, Sun Yat-sen University, Guangzhou 510060, China

Received November 26, 2019; Revised March 17, 2020; Editorial Decision March 24, 2020; Accepted April 18, 2020

ABSTRACT

ALT tumor cells often contain abundant DNA damage foci at telomeres and rely on the alternative lengthening of telomeres (ALT) mechanism to maintain their telomeres. How the telomere chromatin is regulated and maintained in these cells remains largely unknown. In this study, we present evidence that heterochromatin protein 1 binding protein 3 (HP1BP3) can localize to telomeres and is particularly enriched on telomeres in ALT cells. HP1BP3 inhibition led to preferential growth inhibition of ALT cells, which was accompanied by telomere chromatin decompaction, increased presence of C-circles, more pronounced ALT-associated phenotypes and elongated telomeres. Furthermore, HP1BP3 appeared to participate in regulating telomere histone H3K9me3 epigenetic marks. Taken together, our data suggest that HP1BP3 functions on telomeres to maintain telomere chromatin and represents a novel target for inhibiting ALT cancer cells.

INTRODUCTION

Nearly 85–90% of cancer cells are telomerase-positive and rely on telomerase to elongate telomeres. Telomerase-negative cancer cells maintain telomeres through the alternative lengthening of telomeres (ALT) pathway that depends on homologous recombination (HR) (1). Telomerase-positive tumors can also lose telomerase expression and become ALT-like cells (2,3). Structural abnormalities of telomeres and dysfunctional telomere-binding proteins have been well documented in ALT cells (4–7). ALT cells typically exhibit global DNA damage, abnormally heterogeneous telomeres, ALT-associated promyelocytic leukaemia bodies (APBs), extra-chromosomal circular DNA of telomeric repeats (C-circles) and more frequent telomere-sister chromatid exchanges (T-SCE) (8–11). However, the mechanisms underlying ALT activation and maintenance, and ALT tumor development remain largely unknown. ALT tumors are often associated with higher degree of malignancy (2,3), and more difficult to treat clinically (12–14). Blocking ATR activity was reported to inhibit ALT cell growth (15), suggesting that targeting DNA damage response pathways may help combat ALT cancer.

In telomerase-positive cells, telomere chromatin is enriched in repressive histone modifications, including hypoacetylation, HP1 binding and histone H3K9 and H4K20 trimethylation (16–20). For example, HP1α and HP1β are associated with telomeres and subtelomeres, and regulate telomere chromatin compaction (18,21). Unlike telomerase-positive cells, ALT cells present different binding proteins and structures at the telomere chromatin. For instance, telomere chromatin compaction appears reduced in these cells (4). Recently, dysfunction of the chromatin regulating complex components alpha-thalassemia X-linked syndrome protein (ATRX) and death domain-associated protein (DAXX) has been linked to increased ALT features (22–25). A key activity of the DAXX-ATRX complex is to function as a chaperon and deposit H3.3 on telomeres (26). We have previously shown that the DAXX-ATRX complex maintained telomere stability and promoted histone H3K9 methylation at telomeres (27,28). ATRX/DAXX knockdown (KD) could promote the cells

*To whom correspondence should be addressed. Tel: +86 20 39943778; Fax: +86 20 39943778; Email: songyang@bcm.edu
Correspondence may also be addressed to Junjiu Huang. Tel: +86 20 39943778; Fax: +86 20 39943778; Email: hjunjiu@mail.sysu.edu.cn
†The authors wish it to be known that, in their opinion, the first two authors should be regarded as Joint First Authors.

transition from telomerase-positive to more ALT-like (2). However, the integration of epigenetic machineries into the telomere maintenance process and differential regulation of telomere chromatin in ALT versus telomerase-positive cells remain outstanding questions.

Our large-scale immunoprecipitation (IP) and mass spectrometry analysis of DAXX found heterochromatin protein 1 (HP1) and HP1-binding protein 3 (HP1BP3) to associate with DAXX (27,28). Several studies have demonstrated the importance of HP1 to telomere stability and integrity, linking HP1 dysfunction to cancer progression (21,29). Initially identified as a HP1-binding protein, HP1BP3 shares certain similarities with histone H1 structurally and functionally (30). HP1BP3 knockout (KO) in mice resulted in decreased postnatal viability and growth (30). It has since been shown to bind DNA and nucleosomes (30,31), maintain chromatin structure, and regulate transcription (31,32). Here, we show that HP1BP3 can be targeted to telomeres in ALT cells and regulate telomere chromatin compaction by modulating H3K9me3 occupancy and oligomerizing histone H1. These findings suggest HP1BP3-mediated direct and indirect pathways of telomere chromatin regulation and point to HP1BP3 as an alternative target for treating ALT cancer.

MATERIALS AND METHODS

Cell lines and antibodies

All cells were cultured in DMEM supplemented with 10% fetal bovine serum and 100 units/ml penicillin/streptomycin at 37°C and 5% CO_2. Human full-length HP1BP3 cDNA was cloned into pDEST27 (Invitrogen) for GST tagging and pHAGE-based vectors for Flag tagging (Addgene). pET-MBP-His6-based vectors were for MBP tagging (Addgene). HP1 α cDNA was cloned into pHAGE-based vectors for Flag tagging (Addgene). Histone H1C recombinant protein was purchased from company (Sigma, H1917). Cells were reverse transfected with siRNAs for 48–72 h before analysis. The siRNA sequences are:

siHP1BP3-1: 5′-CCAGAAGAGTGGTGCATCA-3′
siHP1BP3-2: 5′-GTCAGGTCCTGGAAGTAAA-3′
siNC: 5′-TTCTCCGAACGTGTCACGT-3′
siSMC5: 5′-GAAGCAAGAUGUUAUAGAA-3′

Antibodies used in the study include: rabbit polyclonal anti-HP1BP3 (generated in the lab), rabbit polyclonal anti-Flag (Sigma, F7425), anti-HA (Sigma, H3663), anti-GAPDH (ABclonal, AC027), anti-TRF2 (Millipore, 05-521), anti-γH2AX (Millipore, 05-636), rabbit polyclonal anti-GST (Abmart, M20007), mouse monoclonal anti-PML (Santa Cruz, sc966), rabbit polyclonal anti-Histone H3 (Abcam, ab1791), rabbit polyclonal anti-H3K9me3 (Abcam, ab8898) and rabbit polyclonal IgG (Millipore, 12-370). Monoclonal anti-TIN2 antibodies were generated in the Songyang lab.

Generating inducible CRISPR/Cas9 KO cells

Inducible HP1BP3 KO U2OS cells were generated as previously described (33). Briefly, U2OS cells expressing tetracycline-inducible Cas9 were infected with lentiviruses encoding sgRNAs targeting HP1BP3. Two different sgRNAs were used in the same cells. KO efficiency was confirmed by immunoblotting and western blotting with anti-HP1BP3 antibodies. Unless otherwise specified, cells were cultured in 1 μg/ml doxycycline for 7 days before analysis. The HP1BP3 sgRNAs sequences are:

sgRNA-1: 5′-CACCGCACAGTTCGACGAATCGGCA-3′
sgRNA-2: 5′-CACCGTCCACCTGCTACTTCGAGTG-3′

Telomere restriction fragment (TRF) and telomere chromatin immunoprecipitation (Telomere-ChIP) assays

TRF and telomere ChIP assays were performed as previously described (34). For TRF assay, genomic DNA was digested with Hinf1 and Rsa1 and then resolved on 0.7% agarose gels. Southern hybridization was carried out with radiolabeled probes and quantified using a Typhoon PhosphorImager (General Electric Company). Average length of telomeres was calculated using TeloRun.

For telomere-ChIP, cells were fixed with 1% formaldehyde was and then sonicated before pre-clearing using protein A/G-agarose beads and control immunoglobulins (IgG) (2 μg). Following incubation with the appropriated antibodies (3 μg), co-precipitated DNA was eluted for slot-blotting and hybridization using radiolabeled or biotinlabeled probes.

Telo probe: 5′-Biotin-TTAGGGTTAGGGTTAGGGT
ALU probe: 5′-Biotin-GGCCGGGCGCGGTGGCTCACGCCTGTAATCCCAGCA

C-circles (CC) assay

CC assay was performed as described previously (9). Genomic DNA was digested with Hinf1 and Rsa1 (4 U/μg) plus RNaseA/T (25 ng/μl) (Dnase-free; Fementas). An aliquot of the digest was used as input. The remaining was diluted to the designed concentration (25, 50 or 100 ng of DNA per 10 μl volume) and combined with 10 μl of reaction mixture (5 μg BSA, 0.1% Tween 20, 1 mM dATP, 1 mM dTTP, 1 mM dGTP, 2 × Φ29 buffer, and 5 U Φ29 DNA polymerase (NEB)), and incubated at 30°C for 4 h followed by 65°C for 20 min. For quantification, 10 μl of final reaction product or input DNA was slot-blotted onto a 2 × SSC-soaked Hybond-N+ membrane. The UV crosslinked membrane was hybridized at 45°C with 5′-labeled TelC probes for Φ29 DNA polymerase amplified product or with ALU probes for input DNA, and visualized using the Chemiluminescent Nucleic Acid Detection Module (Thermo). TelC probe: 5′-Biotin-CCCTAACCCTAACCCTAA. ALU probe: 5′-Biotin-GGCCGGGCGCGGTGGCTCACGCCTGTAATCCCAGCA.

Cell counting kit-8 (CCK-8) assay

Cells viability was assayed with cell counting kit-8 (CCK-8, CK04-500, Dojindo, Kumamoto, Japan). Inducible knockout HP1BP3 U2OS cells and Cas9 inducible expression

U2OS cells were cultured with Doxycycline (1 μg/ml) for 3 days (72 h) and then seeded in 96-well plates (5×10^3/well). Subsequently cells were continuously incubated with Doxycycline (1 μg/ml) at 37°C at 96, 120, 144, 168 h. In addition, U2OS, SAOS2, WI38-VA13, Hela and MG63 cells were seeded in 96-well plates (5×10^3/well) and siRNA was transfected into the cells 24 h later. In the same way, transfected cells were incubated at 37°C for 24, 48, 72 and 96 h. The medium of each well was replaced with 100 μl fresh culture media contained 10% CCK-8 at different times. The 450 nm wavelength absorbance was measured using microplate reader (SYNERGY-HTX multi-mode reader, BioTek).

Chromosome orientation FISH (CO–FISH) assay

CO-FISH was performed as described previously (35). Cells were incubated with BrdU for 19 h before addition of nocodazole for another 6 h. Cells were then collected and washed with 75 mM KCl three times before being fixed with methanol:glacial acetic acid (3:1) and spread onto precleaned slides. The slides were hydrated with 1× PBS before digestion with pepsin solution (1 mg/ml, pH 2.0), and then stained using Hoechst 33258. After UV treatment, the slides were finally treated with Exonuclease III. The slides were next washed twice in sterile water, dehydrated successively with 70%, 90% and 100% ethanol, and then incubated with the Alexa Fluor-488-$(TTAGGG)_3$ for 2 h and denatured at 85°C for 10 s. The slides were subsequently washed with 70% formamide solution, dehydrated successively with 70%, 90% and 100% ethanol, and incubated with the Alexa Fluor-488-$(CCCTAA)_3$ probe for another 2 h. Lastly, the slides were washed and dehydrated before being mounted with DAPI. Photographs were taken on a Zeiss AxioImager Z1 microscopy.

Telomere quantitative fluorescent *in situ* hybridization (Q-FISH)

Cells were cultured with 0.5 μg/ml nocodazole for 6 h before being treated in 75 mM KCl and then fixed in methanol and glacial acetic acid solution (3:1) followed by being spread onto clean slides. Slides were denatured at 85°C for 4 min and hybridized with the FITC-labeled telomere (5-CCCTAA-3) peptide nucleic acid probes (0.5 μg/ml) (Panagene, Korea). Chromosomes were stained with DAPI (0.5 μg/ml). Slides were imaged on a Zeiss microscope with FITC/DAPI filters by AxioCam and AxioVision software 4.8. Telomere fluorescence intensity was integrated using the TFL-TELO program.

Micrococcal nuclease (MNase) assay

Cells were washed twice each with 1× PBS and buffer A (100 mM NaCl, 10 mM Tris [pH 7.5], 3 mM $MgCl_2$, 1 mM $CaCl_2$, 0.5 mM phenylmethylsulfonyl fluoride, and protease inhibitor cocktail), and then resuspended in buffer A plus 0.7% NP-40 and incubated on ice for 5 min. The nuclei were harvested and resuspended in 650 μl buffer A. Each 100 μl sample was incubated with 5 μl micrococcal nuclease (1 U/μl) at 30°C for the intended amount of time before addition of 1 volume (100 μl) of TES-proK (10 mM Tris–HCl [pH 7.5], 10 mM EDTA, 1% SDS, 0.2 mg/ml proteinase K) and incubation overnight at 37°C. DNA was phenol–chloroform extracted and ethanol precipitated, resolved on a 1.5% agarose gel in Tris-acetate EDTA (TAE) buffer, transferred to the Hybrid XL membrane, and hybridized with isotope labeled probes.

In vitro peptide pull-down assay

Unmodified and modified (H3K4me3 or H3K9me3) biotinylated histone H3 tail peptides (a.a. 1–21) were purchased from Millipore. Hela cells stably expressing Flag-tagged HP1BP3 or HP1 were used for anti-Flag IP. The immunoprecipitates were then used for *in vitro* pull-down assays with the H3 peptides as described previously (36).

Immunoprecipitation *In vitro* pull-down assays

Whole cell extracts from HEK293T cells expressing the GST-HP1BP3 and SFB-tagged HP1BP3 were incubated with glutathione resin for the GST pull-down assay, followed by western blotting using the appropriate antibodies.

RESULTS

Telomeric localization of HP1BP3 is enriched in ALT cells

Given that both DAXX and HP1 participate in telomere regulation, we speculated that HP1BP3 might also interact with telomeric proteins and target to telomeres. When we co-expressed Flag-tagged HP1BP3 with GST-tagged TRF1 or TRF2 in 293T cells, anti-Flag immunoprecipitation (IP) of HP1BP3 brought down both TRF1 and TRF2, suggesting interactions between HP1BP3 and core telomere proteins (Figure 1A, Up). Furthermore, we purified MBP-HP1BP3 protein and carried out pull down assay to test whether HP1BP3 interacted with TRF2 TRFH domain. Our data showed that HP1BP3 interacted with TRF2 TRFH domain but not TRF2 ΔTRFH, indicating HP1BP3-TRF2 interaction was dependent on TRF2 TRFH domain (Supplementary Figure S1A, Figure 1A Down). Next, we carried out telomere ChIP assays using U2OS cells expressing Flag-tagged HP1BP3 or HP1α (Supplementary Figure S1B) and observed that Flag ChIP of HP1BP3 and HP1 brought down telomere DNA. To better determine telomere localization of endogenous HP1BP3, we generated an anti-HP1BP3 antibody and showed this antibody could specifically recognized endogenous HP1BP3 by western blotting and immunostaining (Supplementary Figure S1C, D). Indeed, anti-HP1BP3 ChIP brought down telomere DNA (Figure 1B, C), suggesting telomeric targeting of HP1BP3. Furthermore, ChIP analysis was carried out in HP1BP3 knocked down (KD) cells using two different siRNAs and anti-HP1BP3 antibody, and we observed that a decrease of HP1BP3 telomere binding in HP1BP3 KD cells (Figure 1D, E).

We then examined endogenous HP1BP3 localization in both telomerase-positive (HTC75 and Hela229) and ALT

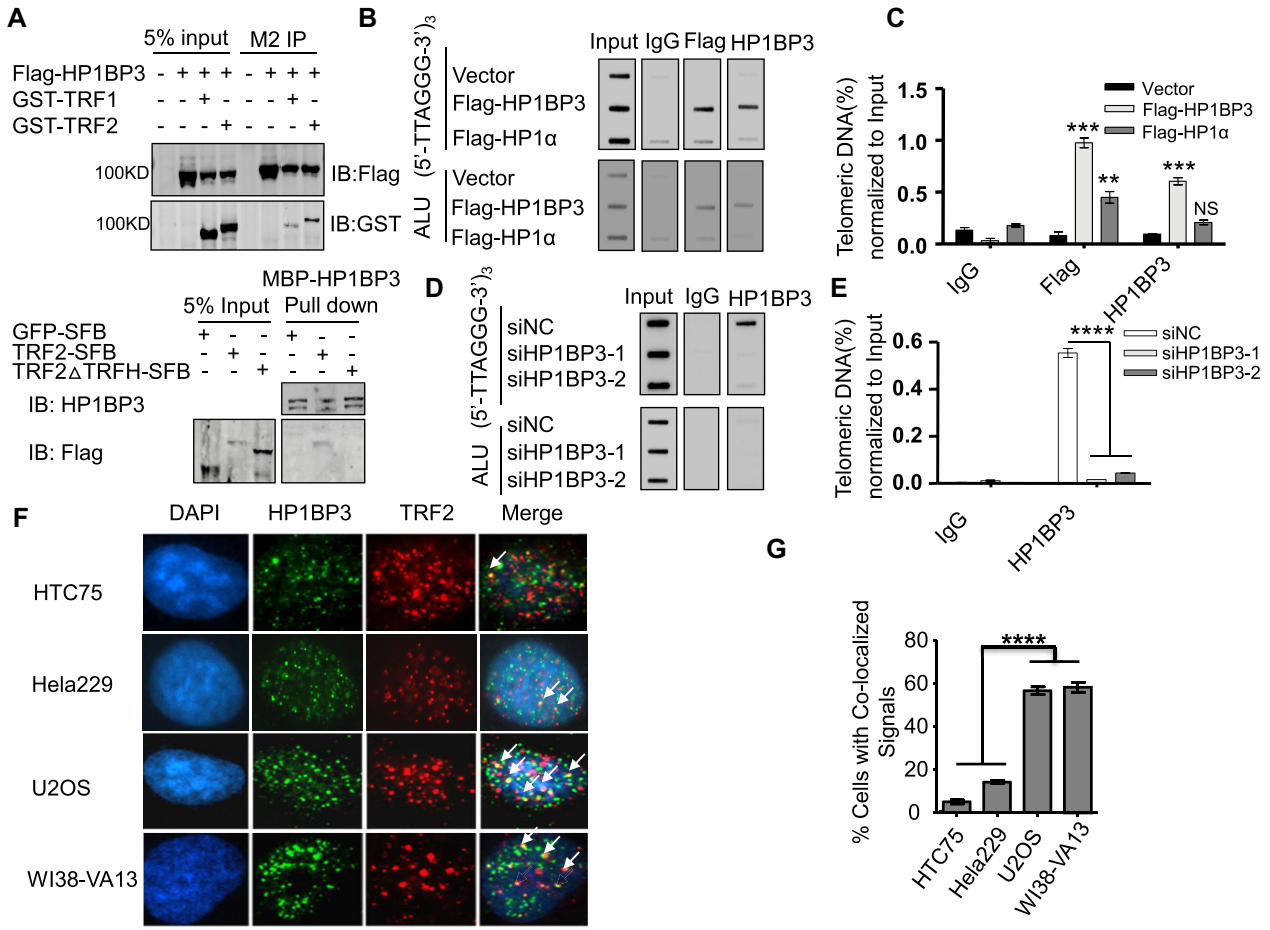

Figure 1. HP1BP3 can localize to telomeres in both telomerase-positive and ALT cells. (**A**) 293T cells transiently co-expressing Flag-HP1BP3 together with GST-tagged TRF1 or TRF2 were harvested for co-immunoprecipitation experiments using an anti-Flag antibody. The IP products were resolved by SDS-PAGE and western blotted as indicated (Up). MBP-HP1BP3 protein was purified *in vitro*. Pull down assay was carried out to detect HP1BP3 interacted with SFB tagged TRF2 and TRF2 ΔTRFH from cells expressing lysis. Then WB analysis was detected using Flag and HP1BP3 antibodies (Down). (**B**) U2OS cells stably expressing vector alone, Flag-HP1BP3, or Flag-HP1 were used in telomere ChIP assays with anti-IgG, anti-Flag and anti-HP1BP3 antibodies. The precipitated DNA was slot-blotted and probed with a biotinylated telomere probe $(5'\text{-TTAGGG-}3')_3$. An ALU probe was used to control for input and IgG served as a negative control. (**C**) Signals from (B) were quantified and normalized either to input. Error bars represent mean±SD; n = 3 independent experiment. $^{***}P < 0.001$, $^{**}P < 0.01$, NS, not significant (two-tailed *t* test). (**D**) U2OS cells were transiently transfected with two different siRNAs that target HP1BP3 and then harvested for telomere ChIP assays using anti-IgG and anti-HP1BP3 antibodies. siNC, non-silencing control siRNA. ChIPed DNA was slot-blotted as described in (B). (**E**) Signals from (D) were quantified and normalized either to input. Error bars represent mean ± SD; *n* = 3 independent experiment. $^{****}P < 0.0001$ (two-tailed *t* test). (**F**) Immunofluorescence (IF) was carried out using anti-HP1BP3 (green) and TRF2 (red) antibodies in telomerase-positive (HTC75 and Hela229) and ALT (U2OS and WI38-VA13) cells. DAPI was used to stain nuclei. White arrows indicate co-localized signals. (**G**) Data from (F) were quantified and plotted. Cells with ≥3 co-localized foci were counted as positive. At least 200 cells were examined for each line. mean ± SD, *n* = 3 independent experiments, $^{****}P < 0.0005$ (two-tailed *t* test).

(U2OS and WI38-VA13) cells (Figure 1F). As expected, TRF2 staining exhibited the characteristic punctate pattern. Partial overlapping signals of HP1BP3 and TRF2 staining could be observed in all the lines tested, supporting co-localization of HP1BP3 and telomeric proteins. Compared to the telomerase-positive cells, U2OS and WI38-VA13 displayed considerably more HP1BP3/TRF2 co-staining foci (Figure 1G), possibly because the disproportionately long telomeres in these ALT cells provided more protein-binding sites (Supplementary Figure S1E, F). Taken together, these results indicate that HP1BP3 can localize to telomeres regardless of telomerase status, but may be more enriched at telomeres in ALT cells.

HP1BP3 knockdown induces telomere DNA damage responses

When the HP1BP3 KD cells (Supplementary Figure S2A) were further examined, we noticed the proliferation of the ALT cells (U2OS, SAOS2 and WI38VA13) was markedly inhibited, whereas that of the telomerase-positive Hela and MG63 cells was only moderately affected as measured by direct cell counting (Figure 2A). Because SAOS2 cells lack p53, inhibition of ALT cell growth by HP1BP3 KD is likely p53 independent. Cell counting kit-8 (CCK-8) assay confirmed that growth of HP1BP3 depleting ALT cells was inhibited (Figure 2B), suggesting increased sensitivity of ALT cells upon HP1BP3 inhibition.

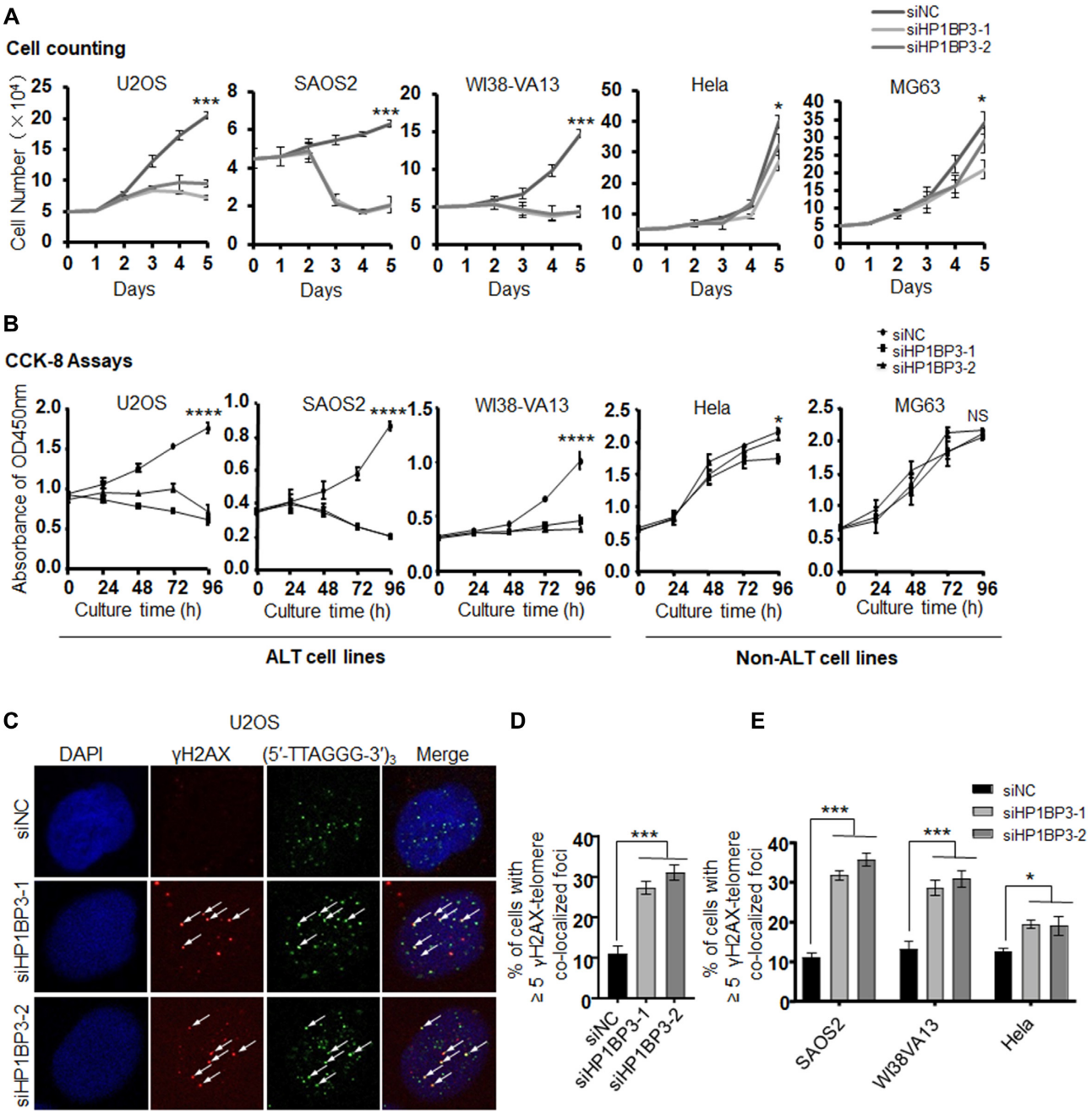

Figure 2. HP1BP3 inhibition induces DNA damage response at telomeres. (**A**) Approximately 5×10^4 cells for each cell line (U2OS, SAOS2,WI38VA13,HeLa and MG63) were seeded at day 0 (D0) and transfected with control (siNC) or HP1BP3 siRNAs at D1. Cell growth was assessed for 5 days and plotted as shown. Error bars represent mean ± SD ($n = 3$ experimental repeats). ***$P < 0.001$, *$P < 0.05$ (two-tailed t test). (**B**) Approximately 5×10^3 cells for each cell line (U2OS, SAOS2, WI38VA13, HeLa and MG63) were seeded at 0 h and transfected with control (NC) or HP1BP3 siRNAs at 24 h. CCK8 assays were carried out to detect the absorbance of $OD_{450\,nm}$ for 96 h. Error bars represent mean ± SD ($n = 3$ experimental repeats). ****$P < 0.0001$, *$P < 0.05$, NS, not significant (two-tailed t test). (**C**) U2OS cells transfected with control (siNC) or two different siRNAs against HP1BP3 were analyzed by IF-FISH with a telomere probe (green) and anti-γH2AX antibodies (red). DAPI was used to stain the nuclei. Arrows indicate co-stained signals. (**D**) The data from (C) were quantified and plotted. About 200 cells were analyzed and those with ≥5 γH2AX-telomere co-localized foci were counted as positive (mean ± SD, $n = 3$ independent experiments). ***$P < 0.0005$ (two-tailed t test). (**E**) SAOS2, WI38VA13 and Hela cells were treated and stained as described in (C), the data were quantified and plotted. About 200 cells were analyzed and those with ≥5 γH2AX-telomere co-localized foci were counted as positive (mean ± SD, $n = 3$ independent experiments). ***P for SAOS2 < 0.00005, ***P for WI38VA13 < 0.0005, *P for HeLa < 0.05 (two-tailed t test).

We went on to co-stain the U2OS HP1BP3 KD cells for γH2AX and telomeres by IF-FISH to evaluate telomere dysfunction induced foci (TIFs). We observed increased TIFs in the HP1BP3 KD cells compared with negative controls, which indicated activation of DNA damage response pathways at telomeres upon HP1BP3 depletion (Figure 2C, D). Similarly, we found that TIFs increased in other cell lines (SAOS2, WI38VA13 and Hela) when KD HP1BP3 (Figure 2E and Supplementary Figure S2B–D).

In fact, a subset of the HP1BP3 KD cells contained micronuclei that stained strongly for γH2AX, even though γH2AX signals were relatively weak elsewhere in the nucleus (Supplementary Figure S2E). Genome instability in ALT cells often leads to micronucleation, which is thought to result from chromosomal missegregation (25). Indeed, while the level of micronucleation itself was unaffected by HP1BP3 KD, an increase in the percentage of cells with micronuclei that co-stained for γH2AX and telomeres was readily apparent (Supplementary Figure S2F), an indication of heightened telomere instability in ALT cells depleted of HP1BP3.

HP1BP3 inhibition promotes ALT activity and elongates telomeres

DNA damage response pathways are intimately linked to telomere maintenance in ALT cells (37,38). In ALT cells and tumors, PNBs (promyelocytic leukaemia bodies) that contain telomeric DNA and proteins (APBs), C-circles, and frequent telomere-sister chromatid exchanges (T-SCE) can be easily detected. In HP1BP3 KD U2OS cells (Supplementary Figure S3A), C-circle formation significantly increased (Figure 3A, B). In contrast, KD of the structural maintenance of chromosomes protein 5 (SMC5), a core component of the SMC5–SMC6 complex that is involved in HR-directed repair of DNA double-strand breaks (DSBs) and telomere recombination (39), had little effect on C-circle formation. In addition, C-circle formation significantly was increased in HP1BP3 KD WI38VA13 cells (Supplementary Figure S3B and Figure 3C). Furthermore, both the number of APBs per cell and the percentages of cells with APBs increased dramatically in HP1BP3 KD U2OS, SAOS2 and WI38VA13 cells (Figure 3D–F and Supplementary Figure S3C, D).

To better investigate the function of HP1BP3, we established inducible HP1BP3 knockout (KO) U2OS cells, in which Cas9 expression was under the control of a tetracycline-responsive promoter and the HP1BP3-targeting sgRNAs were constitutively expressed (33). Upon induction of Cas9 expression, efficient HP1BP3 deletion could be observed (Figure 3G and Supplementary Figure S3E). We then performed chromosome-orientation FISH (CO-FISH) to detect possible changes in T-SCE with HP1BP3 KO (Figure 3H). Consistent with increased C-circles and APBs in HP1BP3 KD cells, HP1BP3 KO also led to more T-SCE (Figure 3I). In HP1BP3 KO cells, we found that HP1BP3 KO decreased cell growth (Supplementary Figure S3F and Figure 3J) and increased TIFs (Figure 3K, L), C-circles formation (Figure 3M, N), and APBs (Supplementary Figure S3G and Figure 3O). These observations point to more pronounced ALT phenotypes upon HP1BP3 inhibition. However, HP1BP3 knockdown increased telomere DNA damage and inhibited ALT cells growth. It supported the notion that HP1BP3 inhibition disrupts telomere maintenance in ALT cells.

Next, we investigated the HP1BP3 KO cells by telomere quantitative fluorescent *in situ* hybridization (Q-FISH). Following Cas9 induction and HP1BP3 KO, stronger telomere signals (∼10% increase in length) could be detected compared to control cells (Figure 3P, Q). These results are similar to what we obtained using HP1BP3 KD cells (Supplementary Figure S4), adding additional evidence that HP1BP3 is important for telomere length regulation in ALT cells.

HP1BP3 knockdown decondenses telomere chromatin in ALT cells

In Hela cells, the KD of HP1BP3 did not affect global chromatin compaction as assayed by nuclease digestion (40). The chromatin is less compacted in ALT cells compared to telomerase-positive cells (4). Given our data that HP1BP3 appeared enriched on telomere chromatin in ALT cells and its loss more severely affected ALT cells, we speculated that the loss of HP1BP3 in ALT cells might lead to the telomere chromatin being further decondensed. To address this possibility, we performed the micrococcal nuclease digestion assay. As expected, prolonged incubation with micrococcal nucleases resulted in the accumulation of smaller telomeric nucleosomes (Figure 4). Compared to control cells, HP1BP3 KD WI38VA13 cells exhibited a specific increase of telomeric but not ALU repeat mono- or di- nucleosomes (Figure 4A–C), indicating decompacted telomeric chromatin. Further analysis revealed both faster enzyme digestion kinetics and more single nucleosomes with HP1BP3 inhibition (Figure 4D, E). Consistent with these findings, HP1BP3 KO or KD U2OS cells again exhibited a specific increase of telomeric but not ALU repeat mono- or di- nucleosomes (Figure 4F–H, and Supplementary Figure S5). Further analysis revealed both faster enzyme digestion kinetics and more single nucleosomes with HP1BP3 inhibition (Figure 4I, J). These results underline the importance of HP1BP3 in telomeric chromatin compaction in ALT cells.

HP1BP3 affects H3K9me3 occupancy on telomeric chromatin in ALT cells

Telomere chromatin is enriched in repressive H3K9me3 modifications and modulated by DAXX (28), HP1α, and SETDB1 (19,20,26). HP1 can bind tri-methylated H3K9 and interact with SETDB1 that generates H3K9me3 marks on telomeres (20,26). Given the association of HP1BP3 with DAXX and HP1 and its telomere targeting, we reasoned that HP1BP3 might also play a role in H3K9me3 modifications of telomere chromatin. Indeed, in U2OS cells ectopically expressing HP1BP3, total level of H3K9me3 increased compared to controls (Figure 5A). This total increase was accompanied by more telomeric recruitment of HP1BP3 (Figure 5B, C) and telomere H3K9me3 marks (Figure 5B and D).

To further confirm the function of HP1BP3 in regulating H3K9me3 on telomeres, we again turned to the inducible

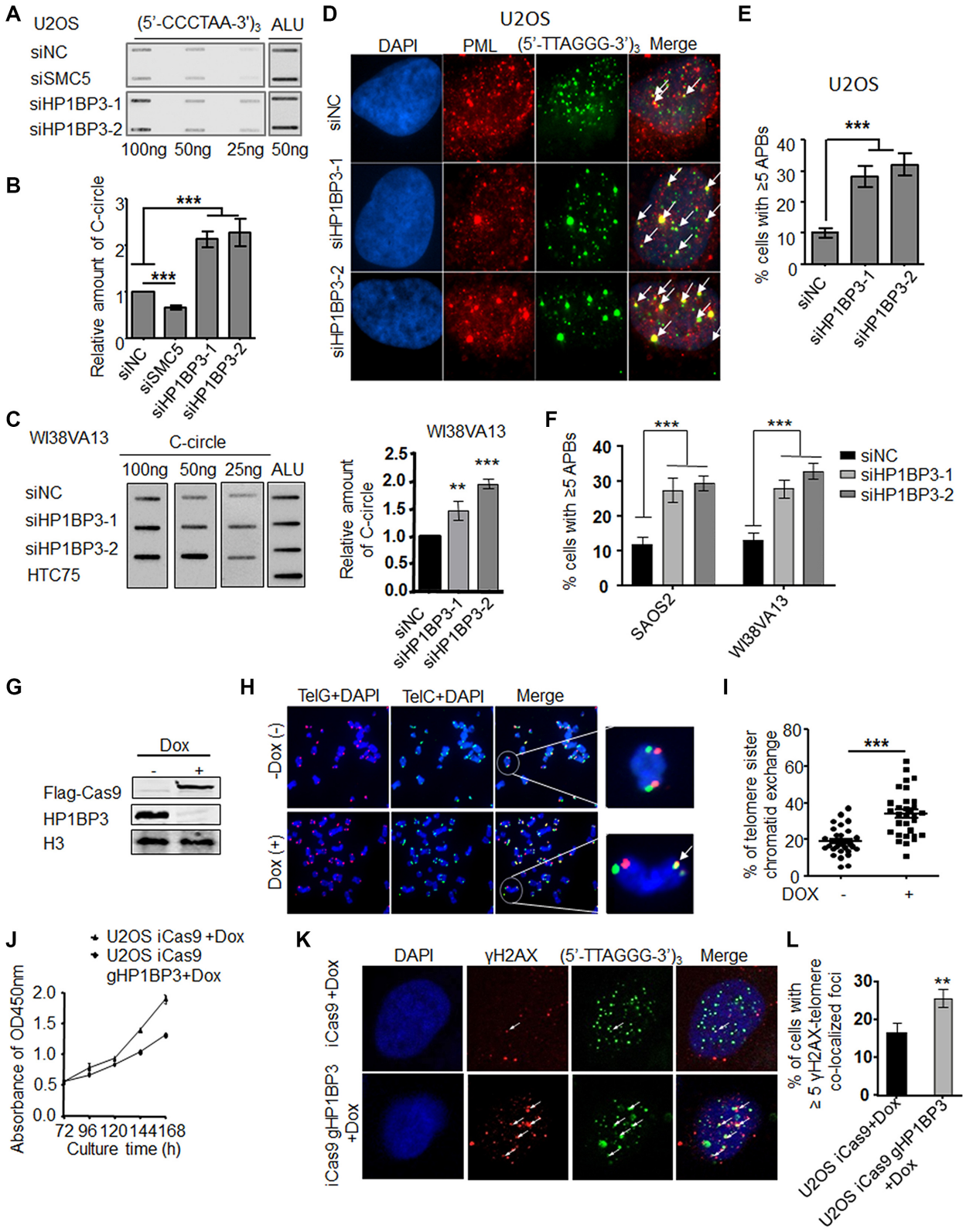
A
U2OS
(5'-CCCTAA-3')3
ALU
siNC
siSMC5
siHP1BP3-1
siHP1BP3-2
100ng 50ng 25ng 50ng
B
Relative amount of C-circle
***
***
siNC
siSMC5
siHP1BP3-1
siHP1BP3-2
C
WI38VA13
C-circle
100ng 50ng 25ng ALU
siNC
siHP1BP3-1
siHP1BP3-2
HTC75
WI38VA13
Relative amount of C-circle
**
***
siNC
siHP1BP3-1
siHP1BP3-2
D
U2OS
DAPI
PML
(5'-TTAGGG-3')3
Merge
siNC
siHP1BP3-1
siHP1BP3-2
E
U2OS
% cells with ≥5 APBs
***
siNC
siHP1BP3-1
siHP1BP3-2
F
% cells with ≥5 APBs
***
***
siNC
siHP1BP3-1
siHP1BP3-2
SAOS2
WI38VA13
G
Dox
- +
Flag-Cas9
HP1BP3
H3
H
TelG+DAPI
TelC+DAPI
Merge
-Dox (-)
Dox (+)
I
% of telomere sister chromatid exchange
***
DOX - +
J
U2OS iCas9 +Dox
U2OS iCas9 gHP1BP3+Dox
Absorbance of OD450nm
72 96 120 144 168
Culture time (h)
K
DAPI
γH2AX
(5'-TTAGGG-3')3
Merge
iCas9 +Dox
iCas9 gHP1BP3 +Dox
L
% of cells with ≥ 5 γH2AX-telomere co-localized foci
**
U2OS iCas9+Dox
U2OS iCas9 gHP1BP3 +Dox

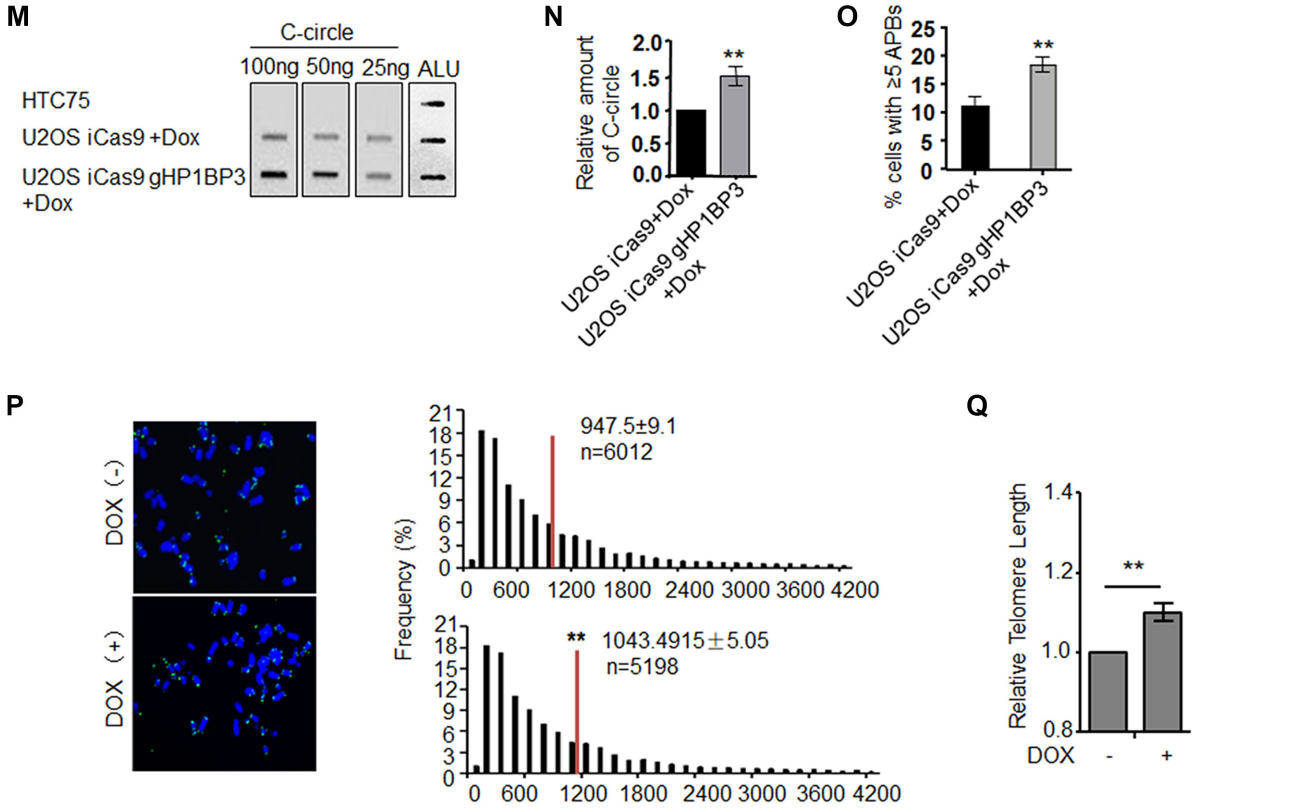

Figure 3. HP1BP3 inhibition enhances ALT activity and elongates telomeres in ALT cells. (**A**) Genomic DNA (25, 50 or 100 ng) from control and siRNA-treated U2OS cells were used for the C-circle assay using a biotin-labeled telomeric probe (5′-CCCTAA-3)$_3$. An ALU repeat probe served as input control. (**B**) Data from (A) were quantified (mean ± SD, $n = 2$ independent experiments). ***$P < 0.001$ (two-tailed t test). (**C**) Genomic DNA (25, 50 or 100 ng) from control and HP1BP3 siRNAs-treated WI38VA13 cells were used for the C-circle assay. Data from (C) were quantified (mean ± SD, $n = 3$ independent experiments). ***$P < 0.001$, **$P < 0.01$ (two-tailed t test). (**D**) IF-FISH analysis of HP1BP3 KD U2OS cells was performed using a telomere PNA-TelC-FITC probe (green) and antibodies against PML (red). DAPI was used to stain nuclei. White arrows indicate superimposable signals. (**E**) Results from (D) were quantified. About 200 cells each lane were counted and those with ≥5 APBs were scored as positive (mean ± SD, $n = 3$ independent experiments). ***$P < 0.001$ (two-tailed t test). (**F**) IF-FISH analysis of HP1BP3 KD SAOS2 and WI38VA13 were carried out as described in (D). Results were quantified. About 200 cells each lane were counted and those with ≥5 APBs were scored as positive (mean ± SD, $n = 3$ independent experiments). ***$P < 0.0005$ (two-tailed t test). (**G**) Inducible HP1BP3 knockout (KO) U2OS cells were generated using two distinct sgRNAs targeting the HP1BP3 gene. Cells treated with (+) or without (−) doxycycline (Dox) for 7 days were analyzed by western blotting with the indicated antibodies. Histone H3 served as a loading control for western blotting. (**H**) Induced HP1BP3 KO cells from (G) were subjected to CO-FISH analysis using TelG (red) and TelC (green) probes. Examples of aberrant telomeres are shown in enlarged images. Arrow indicates exchange events (one chromatid). (**I**) Results from (H) were quantified. At least 30 cells were analyzed for each condition. Error bars indicate standard error ($n = 3$). (mean ± SD, $n = 3$ independent experiments, *** $P < 0.001$ (two-tailed t test). (**J**) Inducible Cas9 only and HP1BP3 KO U2OS cells treated with doxycycline (Dox) for 7 days (about 168 h) were analyzed by western blotting (at 72 h) or CCK-8 assays (72, 96, 120, 144, 168 h). (**K**) Inducible Cas9 only and HP1BP3 KO U2OS cells treated with doxycycline (Dox) for 7 days were analyzed by IF-FISH with a telomere probe (green) and anti-γH2AX antibodies (red). DAPI was used to stain the nuclei. Arrows indicate co-stained signals. (**L**) The data from (K) were quantified and plotted. About 200 cells were analyzed and those with ≥5 γH2AX-telomere co-localized foci were counted as positive (mean ± SD, $n = 3$ independent experiments). ** $P < 0.01$ (two-tailed t test). (**M**) Genomic DNA (25, 50 or 100 ng) from inducible Cas9 only and HP1BP3 KO U2OS cells were used for the C-circle assay using a biotin-labeled telomeric probe (5′-CCCTAA-3)$_3$. An ALU repeat probe served as input control. (N) Data from (M) were quantified (mean ± SD, $n = 3$ independent experiments). **$P < 0.01$ (two-tailed t test). (**O**) IF-FISH analysis of inducible Cas9 only and HP1BP3 KO U2OS cells was performed using a telomere PNA-TelC-FITC probe (green) and antibodies against PML (red). DAPI was used to stain nuclei. White arrows indicate superimposable signals. Then results were quantified. About 200 cells each lane were counted and those with ≥5 APBs were scored as positive (mean ± SD, $n = 3$ independent experiments). **$P < 0.005$ (two-tailed t test). (**P**) Inducible HP1BP3 KO U2OS cells treated with (+) or without (−) Dox for 6 days were analyzed by Q-FISH (left) with the signals plotted on the right. It show the distribution of relative telomere length expressed as fluorescence intensity (TFU, telomere fluorescence unit), and orange lines mark the mean. n indicates the number of telomere signals. (**Q**) Data from (P) were quantified to assess telomere length. mean ± SD, Error bars indicate standard errors. $n = 3$ independent experiments, **$P < 0.01$ (compared with control by unpaired two-tailed t test).

HP1BP3 KO cells. After doxycycline treatment and Cas9 induction, the induced HP1BP3 KO cells were used for immunoprecipitations with anti-HP1BP3 and anti-H3K9me3 antibodies. Consistent with our findings above, induced KO of HP1BP3 drastically decreased the amount of telomeric DNA brought down by anti-HP1BP3 IP (Figure 5E, F). This decrease was also accompanied by reduced telomere DNA brought down by anti-H3K9me3 IP. Taken together, our findings support a critical role of HP1BP3 in regulating H3K9me3 marks on the telomere chromatin.

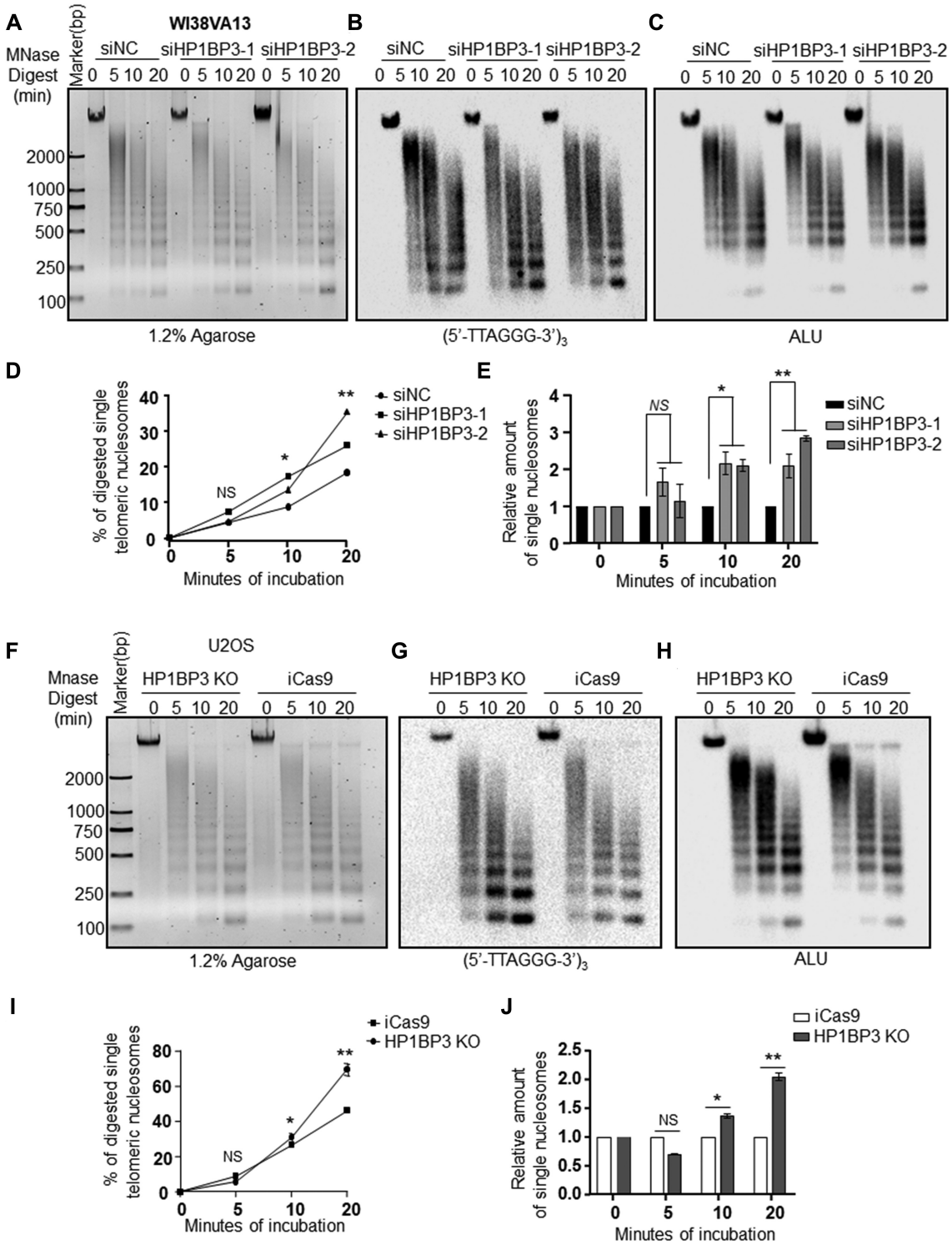

Figure 4. HP1BP3 knockdown or knockout increases the accessibility of telomere chromatin to micrococcal nuclease (MNase). (**A–C**) WI38VA13 cells treated with control and two HP1BP3 siRNAs were lysed and incubated with MNase (5 U) for the indicated amount of time, followed by DNA extraction and southern blot analysis using biotin-labeled telomere and ALU repeat probes. (**D**) Quantitative statistics were obtained by combining the signals in (B, C). The line chart displayed the percentage of telomeric single telomere nucleosomes of HP1BP3 KD vs. siNC single telomere nucleosomes. $^{**}P < 0.01$, $^{*}P < 0.05$, NS, not significant (two-tailed *t* test). (**E**) The histogram displayed the relative amount of telomeric single telomere nucleosomes versus corresponding ALU whole lane. The ratio of 2 min MNase incubation (siNC, siHP1BP3-1 and siHP1BP3-2) was taken as internal parameter. Three independent experiments were performed. (mean ± SD). $^{**}P < 0.01$, $^{*}P < 0.05$, NS, not significant (two-tailed *t* test). (**F–H**) Inducible Cas9 only and HP1BP3 KO U2OS cells were carried out for MNase digestion. Chromatin DNA was extracted and southern blot analysis as described in (A). (**I, J**) Quantitative statistics were obtained as described in (D–F). $^{**}P < 0.01$, $^{*}P < 0.0\,5$, NS, not significant (two-tailed *t* test).

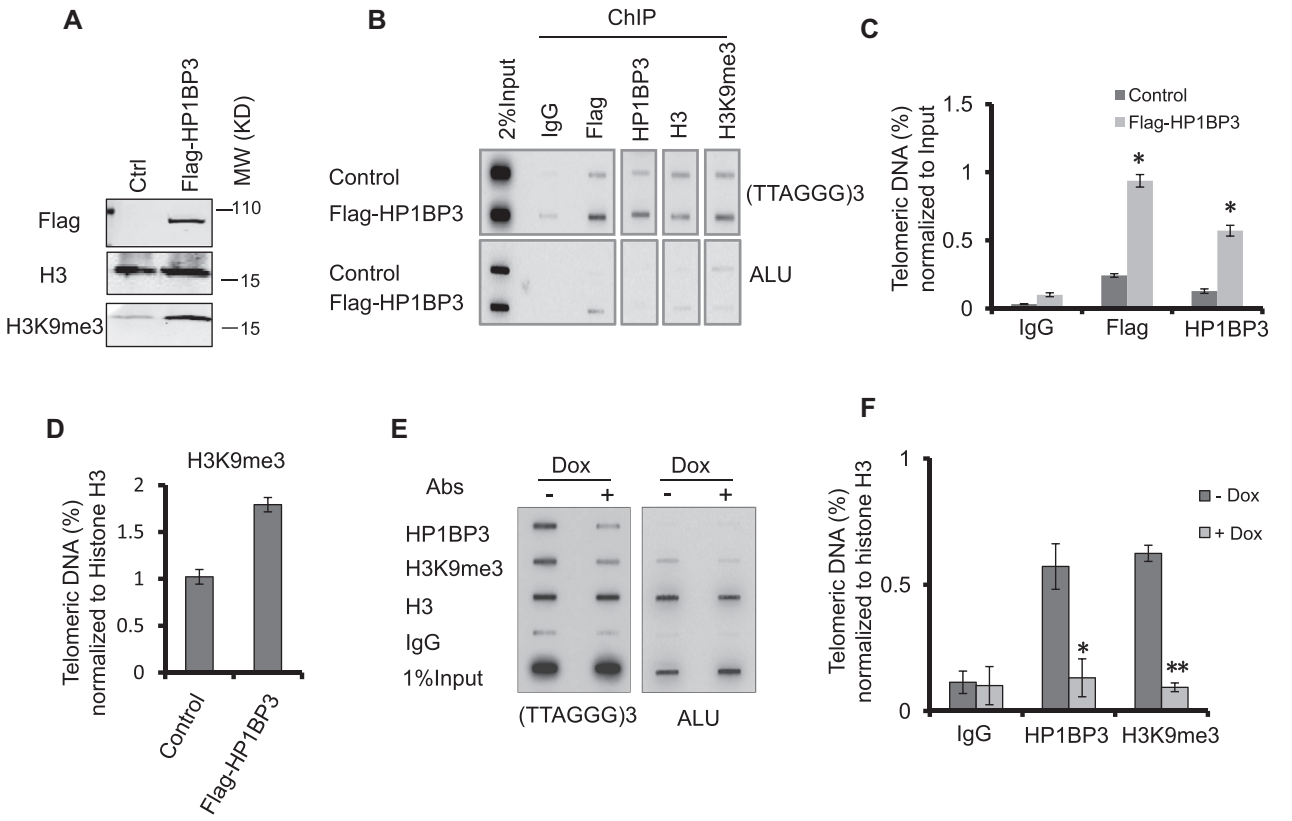

Figure 5. HP1BP3 regulates H3K9me3 occupancy at the telomere chromatin. (**A**) U2OS cells stably expressing vector alone or Flag-tagged HP1BP3 were western blotted as indicated. (**B**) Cells from (A) were used for telomere ChIP analysis with the indicated antibodies. The precipitated DNA was slot blotted and probed with biotin-labeled telomere and ALU probes. Rabbit IgG served as a negative control. (**C, D**) Signals from (B) were quantified and normalized either to input (C) or histone H3 signals (D). Error bars represent mean ± SD; $n = 2$ independent experiment * $P < 0.05$ by unpaired two-tailed t test. (**E**) Inducible HP1BP3 KO U2OS cells treated with (+) or without (−) Dox for 6 days were analyzed by telomere ChIP using the indicated antibodies and processed as in (B). (**F**) Data from (E) were quantified and normalized to histone H3 signals. Error bars represent mean ± SD, Two independent experiments were performed. Significance was calculated using unpaired two-tailed t-test. *$P < 0.05$, **$P < 0.01$.

HP1BP3 can homodimerize and bind multiple copies of histone H1

HP1α is known specifically bind H3K9me3 (41). Indeed, when we used Flag-HP1α expressing cells and biotinylated histone H3 peptides, HP1α could clearly bind to H3K9me3 peptides *in vitro* peptide pull-down assays (Figure 6A). In comparison, when Flag-HP1BP3 was tested in the same assay, both modified and unmodified histone H3 peptides could bring down HP1BP3 (Figure 6A), indicating distinct binding specificities of HP1α versus HP1BP3.

Unlike HP1α, HP1BP3 contains three histone H1 and H5 (H15) domains. As integral components of the chromatin, Histone H1 and H5 do not contain the histone fold motif, functioning as linker histones that bind to internucleosomal DNA and link nucleosomes into higher order structures (30,31,41,42). The H15 domain, a globular ∼80 amino acid region flanked by two less structured tails, is highly conserved in this protein family and essential for H1/H5 binding to the nucleosome. Given the structural and H3 peptide-binding differences between HP1α and HP1BP3, we postulated that the latter might directly bind histones and regulate chromatin independent of HP1α. It is interesting to note that HP1BP3 could also homodimerize. We transiently expressed differently tagged HP1BP3 into 293T cells and found that they could co-IP each other (Figure 6B). With three H15 domains and possible homodimerization, HP1BP3 can in theory associate with multiple copies of histone proteins. To explore this idea further, we carried out *in vitro* pull-down experiments in which different amounts of recombinant H1C proteins (an H1 variant) were mixed with constant amount of bacterially purified MBP-tagged HP1BP3. As shown in Figure 6C, while the level of MBP-HP1BP3 proteins pulled down remained similar, more H1C was co-precipitated as total H1C amount in the reaction increased. Based on the signal intensity of each lane, we estimated that each HP1BP3 protein or protein dimer could bind at least three copies of H1C (Figure 6D), which should allow HP1BP3 to enhance chromatin compaction by increasing H1 access.

DISCUSSION

ALT cancer cells have extensive genome rearrangements, frequent micronucleation, and increased DNA damage foci (25). They depend on DNA damage response pathways to extend telomeres through break-induced replication (37,38). However, excessive telomere DNA damage can induce telomere-driven genome instability (43). Unraveling the mechanisms by which ALT cells proliferate despite the

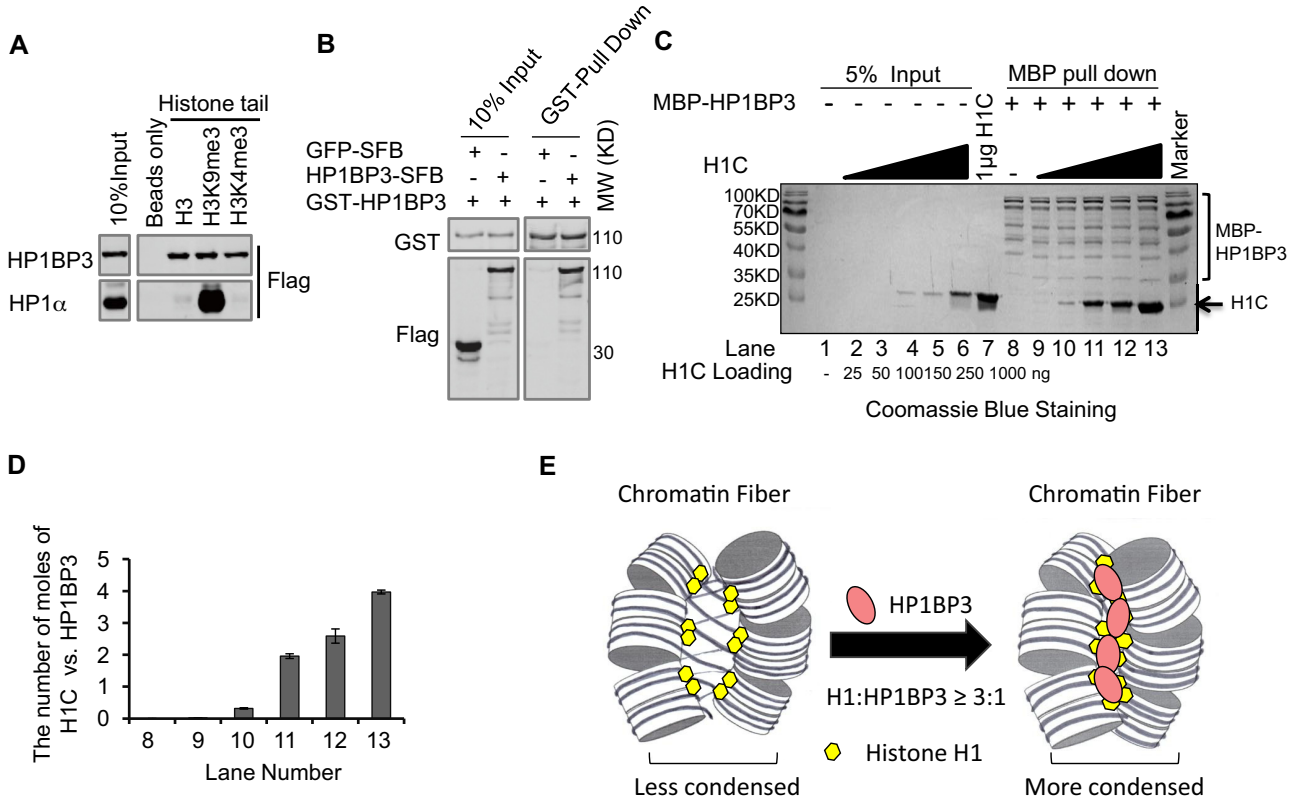

Figure 6. HP1BP3 can homodimerize and oligomerize H1C. (**A**) Lysates from cells expressing Flag-tagged HP1BP3 or HP1α were incubated with biotinylated unmodified and modified (H3K4me3 or H3K9me3) H3 peptides (the first 21 amino acids of the H3 N-terminal tail) followed by strepavidin pull-down and western blotting. (**B**) 293T cells transiently co-transfected with differently tagged HP1BP3 (SFB versus GST) were harvested for GST pull-down and western blotted as indicated. SFB-tagged GFP served as a negative control. (**C**) Constant amount of recombinant MBP-tagged HP1BP3 was incubated with increasing amount of recombinant H1C for the *in vitro* pull-down assay. Bracket indicates all possible MBP-HP1BP3 species. (**D**) Signal intensities of lanes 8–13 were normalized to MBP-HP1BP3 and H1C input and their respective molecular weights to calculate the relative molar ratio of HP1BP3 versus H1C. (**E**) Based on the 30 nm chromatin fiber model and H1-H1 association, binding of HP1BP3 to H1 at a ratio of ≥3:1 should further condense the chromatin fiber.

presence of DNA damage and uncovering the factors that protect their telomere chromatin are central to understanding ALT cancer and telomere regulation in general. Recent evidence suggests that the DAXX-ATRX complex plays an important role in telomere biology and mutations of DAXX and ATRX have been implicated in ALT cancer development (2,23,25,27). We found HP1BP3 to be in the DAXX protein complex and showed here that HP1BP3 could localize to telomeres, especially in ALT cells. DAXX was shown to be preferentially targeted to telomeres in ALT cells (25), perhaps binding to DAXX in turn enriches HP1BP3 on telomeres in ALT cells as well. HP1BP3 can interact with canonical telomeric proteins (e.g., TRF1 and TRF2). Binding of HP1BP3 to TRF2 is dependent on TRF2 TRFH domain. HP1BP3 also interacted with non-telomeric proteins such as histone H1, HP1, and DAXX. We postulate that HP1BP3 likely helped maintain telomere structure and stability in ALT cells. While loss of HP1BP3 was previously reported to have no effect on global chromatin compaction in Hela cells (40), we were able to observe decreased H3K9me3 and less compact chromatin at telomeres as well as increased ALT activity (more C-circles and APBs) upon HP1BP3 inhibition. Recent bioinformatic analysis found enriched H3K9me3 modifications and H3K9me3 methyltransferase SETDB1 at telomeres (20,44). More H3K9me3 modifications can recruit more HP1 and HP1BP3 to compact and silence telomere heterochromatin. It is possible that HP1BP3 may facilitate the crosstalk with methyltramsferase such as SETDB1 for H3K9 trimethylation at telomeres.

Histone H1 could form homodimers and compact nucleosomes through its N terminal globular domain and partial CTD domain (45). H1 and the nucleosome core were shown to associate in 1:1 stoichiometry in a mononucleosome (45). In a 30 nm cryo-EM structure, the nuleosomal units twisted and folded back onto each other to form a left-handed double helix (46). HP1BP3 also contains H15 and CTD domains and can homodimerize. Our *in vitro* binding assay suggests that one HP1BP3 can bind at least three H1C. Given its ability to homodimerize and the presence of three H15 domains, we hypothesize that in addition to regulating H3K9 modifications through HP1, HP1BP3 may directly mediate chromatin compaction, functioning as a super linker histone that clusters multiple H1 proteins for nucleosome condensation.

Compared to telomerase-positive cancer cells, ALT tumor cells have distinct phenotypes and harbor different genetic mutations and epigenetic states (47–50). ALT cancers

tend to more severe and refractory to treatment. Inhibition of DNA repair pathways such as targeting ATR activity has been shown to block ALT cell proliferation (51,52). Here, we report new functions of HP1BP3 and previously unknown mechanisms of telomere chromatin maintenance in ALT cells. In particular, depleting HP1BP3 destabilized telomere chromatin and led to inhibition of proliferation of ALT cells. HP1BP3 has other functions, such as transcription regulation and miRNA processing (53). Although we could not rule out the possibility that altering the expression of other proteins indirectly affected cell growth in HP1BP3 KD cells, we think that regulating telomere chromatin stability by HP1BP3 may be important for tumor cell growth. Our data thus suggest that targeting HP1BP3 or telomere chromatin condensation may constitute a new strategy to combat ALT cancer.

SUPPLEMENTARY DATA

Supplementary Data are available at NAR Online.

ACKNOWLEDGEMENTS

We thank Yuanyan Xiong for help with bioinformatics analysis. We also thank Yan Huang and Feng Liu for comments on the manuscript and helpful discussion.

FUNDING

National Key Research and Development Program of China [2017YFA0102801, 2017YFC1001901]; Science and Technology Planning Project of Guangdong Province [2015B020228002]; National Natural Science Foundation [NSFC 91640119, 31671540, 81330055, 31601196, 31930058]; Natural Science Foundation of Guangdong Province [2016A030310206]; Natural Science Foundation of Guangdong Province [2017A030313093, 201605030012, 201707010085]; Guangdong Basic and Applied Basic Research Foundation [2019A1515011422]. Funding for open access charge: National Key Research and Development Program of China [2017YFA0102801].
Conflict of interest statement. None declared.

REFERENCES

1. Bryan,T.M., Englezou,A., Dalla-Pozza,L., Dunham,M.A. and Reddel,R.R. (1997) Evidence for an alternative mechanism for maintaining telomere length in human tumors and tumor-derived cell lines. *Nat. Med.*, **3**, 1271–1274.
2. Hu,Y., Shi,G., Zhang,L., Li,F., Jiang,Y., Jiang,S., Ma,W., Zhao,Y., Songyang,Z. and Huang,J. (2016) Switch telomerase to ALT mechanism by inducing telomeric DNA damages and dysfunction of ATRX and DAXX. *Sci. Rep.*, **6**, 32280.
3. Hu,J., Hwang,S.S., Liesa,M., Gan,B., Sahin,E., Jaskelioff,M., Ding,Z., Ying,H., Boutin,A.T., Zhang,H. *et al.* (2012) Antitelomerase therapy provokes ALT and mitochondrial adaptive mechanisms in cancer. *Cell*, **148**, 651–663.
4. Episkopou,H., Draskovic,I., Van Beneden,A., Tilman,G., Mattiussi,M., Gobin,M., Arnoult,N., Londono-Vallejo,A. and Decottignies,A. (2014) Alternative lengthening of telomeres is characterized by reduced compaction of telomeric chromatin. *Nucleic Acids Res.*, **42**, 4391–4405.
5. Marzec,P., Armenise,C., Perot,G., Roumelioti,F.M., Basyuk,E., Gagos,S., Chibon,F. and Dejardin,J. (2015) Nuclear-receptor-mediated telomere insertion leads to genome instability in ALT cancers. *Cell*, **160**, 913–927.
6. Conomos,D., Reddel,R.R. and Pickett,H.A. (2014) NuRD-ZNF827 recruitment to telomeres creates a molecular scaffold for homologous recombination. *Nat. Struct. Mol. Biol.*, **21**, 760–770.
7. O'Sullivan,R.J. and Almouzni,G. (2014) Assembly of telomeric chromatin to create ALTernative endings. *Trends Cell Biol.*, **24**, 675–685.
8. Yeager,T.R., Neumann,A.A., Englezou,A., Huschtscha,L.I., Noble,J.R. and Reddel,R.R. (1999) Telomerase-negative immortalized human cells contain a novel type of promyelocytic leukemia (PML) body. *Cancer Res.*, **59**, 4175–4179.
9. Henson,J.D., Cao,Y., Huschtscha,L.I., Chang,A.C., Au,A.Y., Pickett,H.A. and Reddel,R.R. (2009) DNA C-circles are specific and quantifiable markers of alternative-lengthening-of-telomeres activity. *Nat. Biotechnol.*, **27**, 1181–1185.
10. Londono-Vallejo,J.A., Der-Sarkissian,H., Cazes,L., Bacchetti,S. and Reddel,R.R. (2004) Alternative lengthening of telomeres is characterized by high rates of telomeric exchange. *Cancer Res.*, **64**, 2324–2327.
11. Min,J., Wright,W.E. and Shay,J.W. (2017) Alternative lengthening of telomeres can be maintained by preferential elongation of lagging strands. *Nucleic Acids Res.*, **45**, 2615–2628.
12. Costa,A., Daidone,M.G., Daprai,L., Villa,R., Cantu,S., Pilotti,S., Mariani,L., Gronchi,A., Henson,J.D., Reddel,R.R. *et al.* (2006) Telomere maintenance mechanisms in liposarcomas: association with histologic subtypes and disease progression. *Cancer Res.*, **66**, 8918–8924.
13. Chibon,F., Lagarde,P., Salas,S., Perot,G., Brouste,V., Tirode,F., Lucchesi,C., de Reynies,A., Kauffmann,A., Bui,B. *et al.* (2010) Validated prediction of clinical outcome in sarcomas and multiple types of cancer on the basis of a gene expression signature related to genome complexity. *Nat. Med.*, **16**, 781–787.
14. Deeg,K.I., Chung,I., Bauer,C. and Rippe,K. (2016) Cancer cells with alternative lengthening of telomeres do not display a general hypersensitivity to ATR Inhibition. *Front. Oncol.*, **6**, 186.
15. Flynn,R.L., Cox,K.E., Jeitany,M., Wakimoto,H., Bryll,A.R., Ganem,N.J., Bersani,F., Pineda,J.R., Suva,M.L., Benes,C.H. *et al.* (2015) Alternative lengthening of telomeres renders cancer cells hypersensitive to ATR inhibitors. *Science*, **347**, 273–277.
16. Michishita,E., McCord,R.A., Berber,E., Kioi,M., Padilla-Nash,H., Damian,M., Cheung,P., Kusumoto,R., Kawahara,T.L., Barrett,J.C. *et al.* (2008) SIRT6 is a histone H3 lysine 9 deacetylase that modulates telomeric chromatin. *Nature*, **452**, 492–496.
17. Blasco,M.A. (2007) The epigenetic regulation of mammalian telomeres. *Nat. Rev. Genet.*, **8**, 299–309.
18. Lachner,M., O'Carroll,D., Rea,S., Mechtler,K. and Jenuwein,T. (2001) Methylation of histone H3 lysine 9 creates a binding site for HP1 proteins. *Nature*, **410**, 116–120.
19. Kourmouli,N., Sun,Y.M., van der Sar,S., Singh,P.B. and Brown,J.P. (2005) Epigenetic regulation of mammalian pericentric heterochromatin in vivo by HP1. *Biochem. Biophys. Res. Commun.*, **337**, 901–907.
20. Verschure,P.J., van der Kraan,I., de Leeuw,W., van der Vlag,J., Carpenter,A.E., Belmont,A.S. and van Driel,R. (2005) In vivo HP1 targeting causes large-scale chromatin condensation and enhanced histone lysine methylation. *Mol. Cell. Biol.*, **25**, 4552–4564.
21. Fanti,L. and Pimpinelli,S. (2008) HP1: a functionally multifaceted protein. *Curr. Opin. Genet. Dev.*, **18**, 169–174.
22. Pickett,H.A. and Reddel,R.R. (2015) Molecular mechanisms of activity and derepression of alternative lengthening of telomeres. *Nat. Struct. Mol. Biol.*, **22**, 875–880.
23. Napier,C.E., Huschtscha,L.I., Harvey,A., Bower,K., Noble,J.R., Hendrickson,E.A. and Reddel,R.R. (2015) ATRX represses alternative lengthening of telomeres. *Oncotarget*, **6**, 16543–16558.
24. Bower,K., Napier,C.E., Cole,S.L., Dagg,R.A., Lau,L.M., Duncan,E.L., Moy,E.L. and Reddel,R.R. (2012) Loss of wild-type ATRX expression in somatic cell hybrids segregates with activation of alternative lengthening of telomeres. *PLoS One*, **7**, e50062.
25. Lovejoy,C.A., Li,W., Reisenweber,S., Thongthip,S., Bruno,J., de Lange,T., De,S., Petrini,J.H., Sung,P.A., Jasin,M. *et al.* (2012) Loss of ATRX, genome instability, and an altered DNA damage response are hallmarks of the alternative lengthening of telomeres pathway. *PLos Genet.*, **8**, e1002772.
26. Hoelper,D., Huang,H., Jain,A.Y., Patel,D.J. and Lewis,P.W. (2017) Structural and mechanistic insights into ATRX-dependent and

-independent functions of the histone chaperone DAXX. *Nat. Commun.*, **8**, 1193.
27. Tang,M., Li,Y., Zhang,Y., Chen,Y., Huang,W., Wang,D., Zaug,A.J., Liu,D., Zhao,Y., Cech,T.R. *et al.* (2015) Disease mutant analysis identifies a new function of DAXX in telomerase regulation and telomere maintenance. *J. Cell Sci.*, **128**, 331–341.
28. He,Q., Kim,H., Huang,R., Lu,W., Tang,M., Shi,F., Yang,D., Zhang,X., Huang,J., Liu,D. *et al.* (2015) The Daxx/Atrx complex protects tandem repetitive elements during DNA hypomethylation by promoting H3K9 trimethylation. *Cell Stem Cell*, **17**, 273–286.
29. Dialynas,G.K., Vitalini,M.W. and Wallrath,L.L. (2008) Linking heterochromatin protein 1 (HP1) to cancer progression. *Mutat. Res.*, **647**, 13–20.
30. Garfinkel,B.P., Melamed-Book,N., Anuka,E., Bustin,M. and Orly,J. (2015) HP1BP3 is a novel histone H1 related protein with essential roles in viability and growth. *Nucleic Acids Res.*, **43**, 2074–2090.
31. Hayashihara,K., Uchiyama,S., Shimamoto,S., Kobayashi,S., Tomschik,M., Wakamatsu,H., No,D., Sugahara,H., Hori,N., Noda,M. *et al.* (2010) The middle region of an HP1-binding protein, HP1-BP74, associates with linker DNA at the entry/exit site of nucleosomal DNA. *J. Biol. Chem.*, **285**, 6498–6507.
32. Garfinkel,B.P., Arad,S., Le,P.T., Bustin,M., Rosen,C.J., Gabet,Y. and Orly,J. (2015) Proportionate Dwarfism in mice lacking heterochromatin protein 1 binding protein 3 (HP1BP3) is associated with alterations in the endocrine IGF-1 pathway. *Endocrinology*, **156**, 4558–4570.
33. Kim,H., Li,F., He,Q., Deng,T., Xu,J., Jin,F., Coarfa,C., Putluri,N., Liu,D. and Songyang,Z. (2017) Systematic analysis of human telomeric dysfunction using inducible telosome/shelterin CRISPR/Cas9 knockout cells. *Cell Discov.*, **3**, 17034.
34. Feng,X., Luo,Z., Jiang,S., Li,F., Han,X., Hu,Y., Wang,D., Zhao,Y., Ma,W., Liu,D. *et al.* (2013) The telomere-associated homeobox-containing protein TAH1/HMBOX1 participates in telomere maintenance in ALT cells. *J. Cell Sci.*, **126**, 3982–3989.
35. Bailey,S.M., Cornforth,M.N., Kurimasa,A., Chen,D.J. and Goodwin,E.H. (2001) Strand-specific postreplicative processing of mammalian telomeres. *Science*, **293**, 2462–2465.
36. Qiu,J., Shi,G., Jia,Y., Li,J., Wu,M., Li,J., Dong,S. and Wong,J. (2010) The X-linked mental retardation gene PHF8 is a histone demethylase involved in neuronal differentiation. *Cell Res.*, **20**, 908–918.
37. Dilley,R.L., Verma,P., Cho,N.W., Winters,H.D., Wondisford,A.R. and Greenberg,R.A. (2016) Break-induced telomere synthesis underlies alternative telomere maintenance. *Nature*, **539**, 54–58.
38. Cho,N.W., Dilley,R.L., Lampson,M.A. and Greenberg,R.A. (2014) Interchromosomal homology searches drive directional ALT telomere movement and synapsis. *Cell*, **159**, 108–121.
39. Potts,P.R. and Yu,H. (2007) The SMC5/6 complex maintains telomere length in ALT cancer cells through SUMOylation of telomere-binding proteins. *Nat. Struct. Mol. Biol.*, **14**, 581–590.
40. Dutta,B., Ren,Y., Hao,P., Sim,K.H., Cheow,E., Adav,S., Tam,J.P. and Sze,S.K. (2014) Profiling of the chromatin-associated proteome identifies HP1BP3 as a novel regulator of cell cycle progression. *Mol. Cell. Proteomics.***9**, 2183–2197.
41. Nishibuchi,G., Machida,S., Osakabe,A., Murakoshi,H., Hiragami-Hamada,K., Nakagawa,R., Fischle,W., Nishimura,Y., Kurumizaka,H., Tagami,H. *et al.* (2014) N-terminal phosphorylation of HP1alpha increases its nucleosome-binding specificity. *Nucleic Acids Res.*, **42**, 12498–12511.
42. Harshman,S.W., Young,N.L., Parthun,M.R. and Freitas,M.A. (2013) H1 histones: current perspectives and challenges. *Nucleic Acids Res.*, **41**, 9593–9609.
43. Fumagalli,M., Rossiello,F., Clerici,M., Barozzi,S., Cittaro,D., Kaplunov,J.M., Bucci,G., Dobreva,M., Matti,V., Beausejour,C.M. *et al.* (2012) Telomeric DNA damage is irreparable and causes persistent DNA-damage-response activation. *Nat. Cell Biol.*, **14**, 355–365.
44. Cubiles,M.D., Barroso,S., Vaquero-Sedas,M.I., Enguix,A., Aguilera,A. and Vega-Palas,M.A. (2018) Epigenetic features of human telomeres. *Nucleic Acids Res.*, **46**, 2347–2355.
45. Syed,S.H., Goutte-Gattat,D., Becker,N., Meyer,S., Shukla,M.S., Hayes,J.J., Everaers,R., Angelov,D., Bednar,J. and Dimitrov,S. (2010) Single-base resolution mapping of H1-nucleosome interactions and 3D organization of the nucleosome. *PNAS*, **107**, 9620–9625.
46. Song,F., Chen,P., Sun,D., Wang,M., Dong,L., Liang,D., Xu,R.M., Zhu,P. and Li,G. (2014) Cryo-EM study of the chromatin fiber reveals a double helix twisted by tetranucleosomal units. *Science*, **344**, 376–380.
47. Murnane,J.P. (2012) Telomere dysfunction and chromosome instability. *Mutat. Res.*, **730**, 28–36.
48. Turcan,S., Rohle,D., Goenka,A., Walsh,L.A., Fang,F., Yilmaz,E., Campos,C., Fabius,A.W., Lu,C., Ward,P.S. *et al.* (2012) IDH1 mutation is sufficient to establish the glioma hypermethylator phenotype. *Nature*, **483**, 479–483.
49. Sturm,D., Witt,H., Hovestadt,V., Khuong-Quang,D.A., Jones,D.T., Konermann,C., Pfaff,E., Tonjes,M., Sill,M., Bender,S. *et al.* (2012) Hotspot mutations in H3F3A and IDH1 define distinct epigenetic and biological subgroups of glioblastoma. *Cancer Cell*, **22**, 425–437.
50. Schwartzentruber,J., Korshunov,A., Liu,X.Y., Jones,D.T., Pfaff,E., Jacob,K., Sturm,D., Fontebasso,A.M., Quang,D.A., Tonjes,M. *et al.* (2012) Driver mutations in histone H3.3 and chromatin remodelling genes in paediatric glioblastoma. *Nature*, **482**, 226–231.
51. Weber,A.M. and Ryan,A.J. (2015) ATM and ATR as therapeutic targets in cancer. *Pharmacol. Ther.*, **149**, 124–138.
52. Prevo,R., Fokas,E., Reaper,P.M., Charlton,P.A., Pollard,J.R., McKenna,W.G., Muschel,R.J. and Brunner,T.B. (2012) The novel ATR inhibitor VE-821 increases sensitivity of pancreatic cancer cells to radiation and chemotherapy. *Cancer Biol. Ther.*, **13**, 1072–1081.
53. Liu,H., Liang,C., Kollipara,R.K., Matsui,M., Ke,X., Jeong,B.C., Wang,Z., Yoo,K.S., Yadav,G.P., Kinch,L.N. *et al.* (2016) HP1BP3, a chromatin retention factor for Co-transcriptional MicroRNA processing. *Mol. Cell*, **63**, 420–432.